CrossMark
← click for updates

Live Imaging of Host-Parasite Interactions in a Zebrafish Infection Model Reveals Cryptococcal Determinants of Virulence and Central Nervous System Invasion

Jennifer L. Tenor,[a] Stefan H. Oehlers,[b] Jialu L. Yang,[a] ⓘ David M. Tobin,[b] John R. Perfect[a]

Division of Infectious Diseases, Department of Medicine, Duke University Medical Center, Durham, North Carolina, USA[a]; Department of Molecular Genetics and Microbiology, Duke University Medical Center, Durham, North Carolina, USA[b]

J.L.T. and S.H.O. contributed equally to this article.

ABSTRACT The human fungal pathogen *Cryptococcus neoformans* is capable of infecting a broad range of hosts, from invertebrates like amoebas and nematodes to standard vertebrate models such as mice and rabbits. Here we have taken advantage of a zebrafish model to investigate host-pathogen interactions of *Cryptococcus* with the zebrafish innate immune system, which shares a highly conserved framework with that of mammals. Through live-imaging observations and genetic knockdown, we establish that macrophages are the primary immune cells responsible for responding to and containing acute cryptococcal infections. By interrogating survival and cryptococcal burden following infection with a panel of *Cryptococcus* mutants, we find that virulence factors initially identified as important in causing disease in mice are also necessary for pathogenesis in zebrafish larvae. Live imaging of the cranial blood vessels of infected larvae reveals that *C. neoformans* is able to penetrate the zebrafish brain following intravenous infection. By studying a *C. neoformans* FNX1 gene mutant, we find that blood-brain barrier invasion is dependent on a known cryptococcal invasion-promoting pathway previously identified in a murine model of central nervous system invasion. The zebrafish-*C. neoformans* platform provides a visually and genetically accessible vertebrate model system for cryptococcal pathogenesis with many of the advantages of small invertebrates. This model is well suited for higher-throughput screening of mutants, mechanistic dissection of cryptococcal pathogenesis in live animals, and use in the evaluation of therapeutic agents.

IMPORTANCE *Cryptococcus neoformans* is an important opportunistic pathogen that is estimated to be responsible for more than 600,000 deaths worldwide annually. Existing mammalian models of cryptococcal pathogenesis are costly, and the analysis of important pathogenic processes such as meningitis is laborious and remains a challenge to visualize. Conversely, although invertebrate models of cryptococcal infection allow high-throughput assays, they fail to replicate the anatomical complexity found in vertebrates and, specifically, cryptococcal stages of disease. Here we have utilized larval zebrafish as a platform that overcomes many of these limitations. We demonstrate that the pathogenesis of *C. neoformans* infection in zebrafish involves factors identical to those in mammalian and invertebrate infections. We then utilize the live-imaging capacity of zebrafish larvae to follow the progression of cryptococcal infection in real time and establish a relevant model of the critical central nervous system infection phase of disease in a nonmammalian model.

Address correspondence to John R. Perfect, perfe001@mc.duke.edu, or David M. Tobin, david.tobin@duke.edu.

This article is a direct contribution from a Fellow of the American Academy of Microbiology.

As an AIDS-associated pathogen and with an enlarging immuno-suppressed population, *Cryptococcus neoformans* is presently the leading invasive fungal pathogen worldwide by incidence and mortality rates (1). While the disease is initially established in the lung, it is not until it acts on its unique propensity to invade the central nervous system (CNS) that the disease becomes a major life-threatening fungal disease. Clinical presentation most commonly coincides with an established CNS infection, and subsequent mortality rates remain high in both resource-available and resource-limited countries.

Robust but expensive vertebrate model systems such as mice and rabbits have been well established for studying cryptococcal pathogenesis. These models have been effectively used in pathogenesis and treatment studies. For instance, the rabbit model of cryptococcal meningitis, where cryptococci are introduced intracisternally into the subarachnoid space, facilitates dynamic studies of genetic, transcriptional, and biochemical analyses of wild-type and mutant cryptococcal strains during CNS infection (2). The mouse inhalation model allows for detailed evaluation of the host immune response to cryptococcal infection as well as assessment

of cryptococcal virulence determinants of wild-type or mutant strains. However, neither mammalian model allows real-time visualization of the dynamic interaction between innate immune cells and yeasts at distinct sites within the host, and neither model allows easy interrogation of large numbers of wild-type strains and mutants for screening and comparative purposes (3, 4).

Several nonmammalian models of *C. neoformans* pathogenesis have been reported to allow the analysis of cryptococcal pathogenesis through survival and cryptococcal growth assays in invertebrates, namely, *Caenorhabditis elegans* (worm), *Galleria mellonella* (wax moth), and *Drosophila melanogaster* (fruit fly) (5–8). Although these invertebrate models allow rapid analysis of cryptococcal virulence determinants and host genetics to various degrees, there are important limitations. First, the invertebrate nature of these hosts precludes investigations into complex multicellular interactions and specific body sites of infection necessary for investigating processes such as CNS entry and growth within granulomas. Second, anatomical differences between these invertebrate models and mammals limit the information gathered through live imaging of infectious disease progression.

The zebrafish (*Danio rerio*) is a powerful vertebrate model platform that has been applied to investigate host-pathogen interactions. Zebrafish larvae are genetically tractable, optically transparent, and possess several functional organ systems early in development, such as a circulatory system and innate immune system. Infections of zebrafish larvae essentially bridge the technical simplicity of invertebrate models with the tissue and cell type complexity of mammalian models (9). A larval zebrafish model of mucosal *Candida albicans* infection has recently been established. It critically allows the visualization of *Candida*-host interactions at this important but previously unimaged stage of yeast infection. With this basic platform work, the power of zebrafish live-imaging tools for exploring fungal-host interactions was elegantly demonstrated (10).

We propose that live imaging of transparent zebrafish larval will help address key gaps in our knowledge of cryptococcal virulence. Important stages of pathogenesis that are not well understood include the formation of cryptococcomas, the formation *in vivo* of Titan cells, and the mechanism of blood-brain barrier invasion responsible for cryptococcal meningitis—the most dangerous presentation of cryptococcal infection.

Here we have utilized infection of zebrafish larvae to interrogate the host and pathogen genetics that contribute to cryptococcal disease. We find *in vivo* that there is early recruitment of macrophages that phagocytose infecting yeast and provide initial protection. Furthermore, we report the use of hematogenous infection of zebrafish larvae as a simple visual platform for assessing *C. neoformans* invasion across the vertebrate blood-brain barrier and emphasize the relevance of host processes conserved with mammalian immune responses to cryptococcal disease, including macrophages and granulomas.

RESULTS

Macrophages are essential for protecting zebrafish from cryptococcal disease progression. As *C. neoformans* enters a human host, it typically first encounters resident macrophages. Macrophages have been recognized as the primary cell type responsible for containment of *C. neoformans* in experimentally infected mouse lungs (4). To determine whether macrophages play a similar role in a zebrafish model of cryptococcal infection, we assessed the dynamics of macrophage and neutrophil recruitment after injection of fluorescent *C. neoformans* cells into the caudal vein of zebrafish larvae 2 days postfertilization (dpf). To simultaneously image cryptococci, macrophages, and neutrophils, we made use of double transgenic Tg(*lyzC:EGFP*[NZ117], *mfap4:turquoise*[xt27]) animals, in which macrophages are marked by expression of turquoise from the *mfap4* promoter and neutrophils are marked by the expression of enhanced green fluorescent protein (EGFP) from the *lyzC* promoter (11, 12). Macrophages rapidly phagocytosed the majority of *C. neoformans* cells following injection with the majority of injected *C. neoformans* cells observed within *mfap4*-expressing macrophages by 13 h postinfection and only very rare neutrophil phagocytosis of yeast observed during these experiments (Fig. 1A and B). Detailed observation of leukocyte movement around engulfed cryptococcus cells revealed a persistent clustering of macrophages around infected macrophages, consistent with the appearance of a classic cryptococcoma in mammals as primarily composed of macrophages (see Movie S1 in the supplemental material).

Conversely, we observed an initial burst of neutrophils to the site of injection consistent with a response to injection trauma but did not observe clustering or retention of neutrophils around infected macrophages. The defensive role of neutrophils in mammalian models against cryptococcus is unclear. The zebrafish neutrophils appear to be able to recognize *C. neoformans* as foreign but are largely not retained at the site of infection, nor do they appear to be the primary cell type responsible for containment of the yeast. This is likely due to the production of known cryptococcal virulence factors such as capsule (13). In multiple time-lapse experiments, we largely observed macrophage interactions with the yeast. Infrequently, *lyzC*-expressing neutrophils were observed to phagocytose *C. neoformans*. In one example, an *lyzC*-expressing neutrophil phagocytosed *C. neoformans* yeast, migrated away from a nascent granuloma, and was then in turn phagocytosed by an *mfap4*-expressing macrophage nearby a second nascent granuloma (see Movie S2 in the supplemental material). In a second example, we observed a *lyzC*-expressing neutrophil with internalized *C. neoformans* traverse the trunk tissue over 20 h before being phagocytosed by an *mfap4*-expressing macrophage nearby a nascent granuloma (see Movie S3 in the supplemental material). These rare interactions with neutrophils eventually resulted in macrophage engulfment, consistent with a possible role for efferocytosis during the host response to *C. neoformans*.

Serendipitous observation of a Tg(*lyzC:EGFP*[NZ117], *mfap4:turquoise*[xt27]) animal that had been inoculated with *C. neoformans* directly into the trunk vacuole, a fluid-filled tube that is continuous with the brain ventricles, revealed uninhibited *C. neoformans* division in the vacuoles. Our observation suggests that the vacuoles represent an immunologically privileged site as *lyzC*-expressing neutrophils and *mfap4*-expressing macrophages were only recruited to yeast cells residing outside the vacuoles (see Movie S4 in the supplemental material). We hypothesized that the lack of macrophage ingress at these sites allowed the rapid outgrowth of *C. neoformans* not seen in other anatomical sites where macrophages are able to reach and surround the yeasts.

To experimentally test this hypothesis, we depleted zebrafish macrophages by morpholino knockdown of the Spi1/Pu.1 transcription factor (14). As high levels of Pu.1 expression favor macrophage differentiation and intermediate levels favor neutrophil
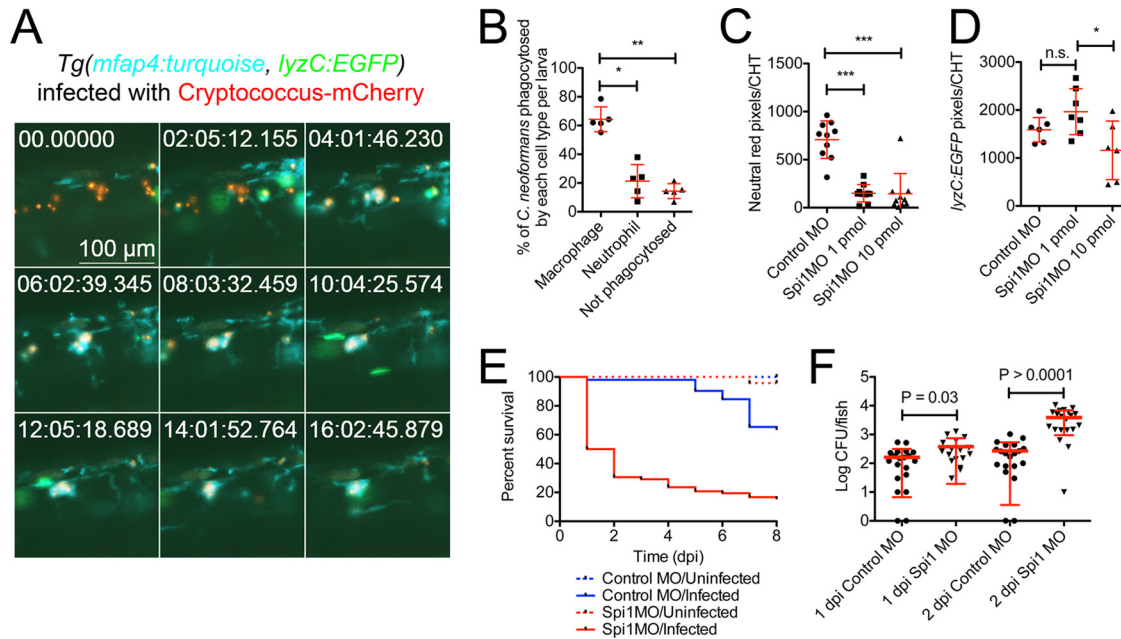
FIG 1 Macrophages are responsible for containing acute *C. neoformans* infection. (A) Still images spaced 2 h apart from time-lapse imaging from a *Tg(lyzC: EGFP^{NZ117}, mfap4:turquoise^{xt27})* larva infected with mCherry-expressing *C. neoformans* starting at 1 h postinfection (neutrophils in green, macrophages in blue, and *Cryptococcus* in red) (full video available as Movie S1 in the supplemental material). The field of view follows a single cluster of yeast cells that are phagocytosed by macrophages by the 4-h mark of the recording. (B) Quantification of the phagocytic fate of *C. neoformans* yeast cells at 13 h postinfection in *Tg(lyzC:EGFP^{NZ117}, mfap4:turquoise^{xt27})* larvae assessed by manual counting. Repeated-measures analysis of variance (ANOVA). The data represent counts from five individual larvae infected with 15 to 30 *C. neoformans* cells each. (C) Quantification of macrophage numbers by fluorescent pixel count in the caudal hematopoietic tissue (CHT) of uninfected 3-dpf larvae injected with a standard dose of 1 pmol and a high dose of 10 pmol Spi1 morpholino (MO) and soaked in neutral red. ANOVA with Tukey posttest. ***, $P < 0.001$. (D) Quantification of neutrophil numbers by fluorescent pixel count in the caudal hematopoietic tissue (CHT) of uninfected 3-dpf *Tg(lyzC:EGFP)* larvae injected with a standard dose of 1 pmol and high dose of 10 pmol Spi1 morpholino. ANOVA with Tukey posttest. *, $P < 0.05$. (E) Survival of Spi1 knockdown larvae following infection with 50 *C. neoformans* cells. Log-rank test between infected conditions. $P < 0.0001$. Data are representative of two experiments each with 15 to 20 larvae per experimental condition. (F) *C. neoformans* burden in Spi1 knockdown larvae at 1 and 2 days postinfection. *t* test. Data are pooled from two experiments each with 10 to 20 larvae per experimental condition.

production, a titrated knockdown of Spi1 with a 1-pmol dose of morpholino arrests myelopoiesis and delays development of macrophages, while neutrophil populations remain largely intact (Fig. 1C and D). Higher doses of morpholino (10 pmol) ablate both macrophage and neutrophil populations (Fig. 1C and D). To test the role of macrophages, we used the lower dose, in which only macrophage development was compromised. These larvae were extremely susceptible to mortality following infection and additionally had a higher fungal burden by 2 days postinfection (dpi), demonstrating a lack of host control of yeast growth (Fig. 1E and F) and, consistent with our *in vivo* imaging studies, implicating macrophages as critical to initial control of infection.

***Cryptococcus neoformans* replicates and establishes persistent infection in zebrafish larvae.** We inoculated 2-dpf zebrafish larvae with a range of *C. neoformans* doses from 20 to 200 yeast cells and observed dose-dependent mortality (Fig. 2A). *C. neoformans* can replicate in zebrafish larvae. The cryptococcal burden was ~2 log CFU higher at 5 dpi than immediately following infection with 50 ± 10 yeast cells (Fig. 2B). The times to death of 50% of larvae (TD$_{50}$s) for infection with 20 ± 5, 50 ± 10, and ~200 yeast cells were 10, 6, and 5 days postinfection, respectively. Thus, inoculum size has an impact on disease, but robust disease and host response can be established with a small burden of yeast cells.

Since macrophages appeared to be the primary intracellular residence of *C. neoformans* in zebrafish larvae, we next performed high-resolution microscopy focusing on yeast cells that were in-

tracellular within macrophages. In spite of the macrophage-dependent restriction of growth, yeast persisted and indeed replicated within macrophages *in vivo* (Fig. 2C; see Movie S5 in the supplemental material). This intracellular division recapitulated the characteristic asymmetrical mother-daughter cell division that can be seen in *in vitro* growth. In addition to expanding capsule diameter, regulation of cell size has been a documented response to conditions experienced during infection by *C. neoformans* (15, 16). Bright-field microscopy of infected larvae suggested that *C. neoformans* increased in size as infection progressed (Fig. 2D). We used an India ink stain to facilitate measurement of capsule diameter and yeast cell sizes. These observations demonstrated an *in vivo* increase in yeast cell body size to the threshold of Titan cell diameter and further the production of capsule enlargement during infection of zebrafish larvae (Fig. 2E, F, and G). This production of capsule is a key characteristic of infection in other animal models and provides a mechanism to explain the observation that *lyzC*-expressing zebrafish neutrophils rarely interact with *C. neoformans* in vivo.

Cryptococcal mutant phenotypes are recapitulated in the zebrafish infection model. The small size and versatility of live-imaging zebrafish larvae make them an ideal host for performing high-throughput host-pathogen interaction screens such as libraries of yeast mutants or multiple mutant or wild-type strains in a mutagenized host platform (17–19). Therefore, to test the robustness of the zebrafish model for mammalian virulence deter-
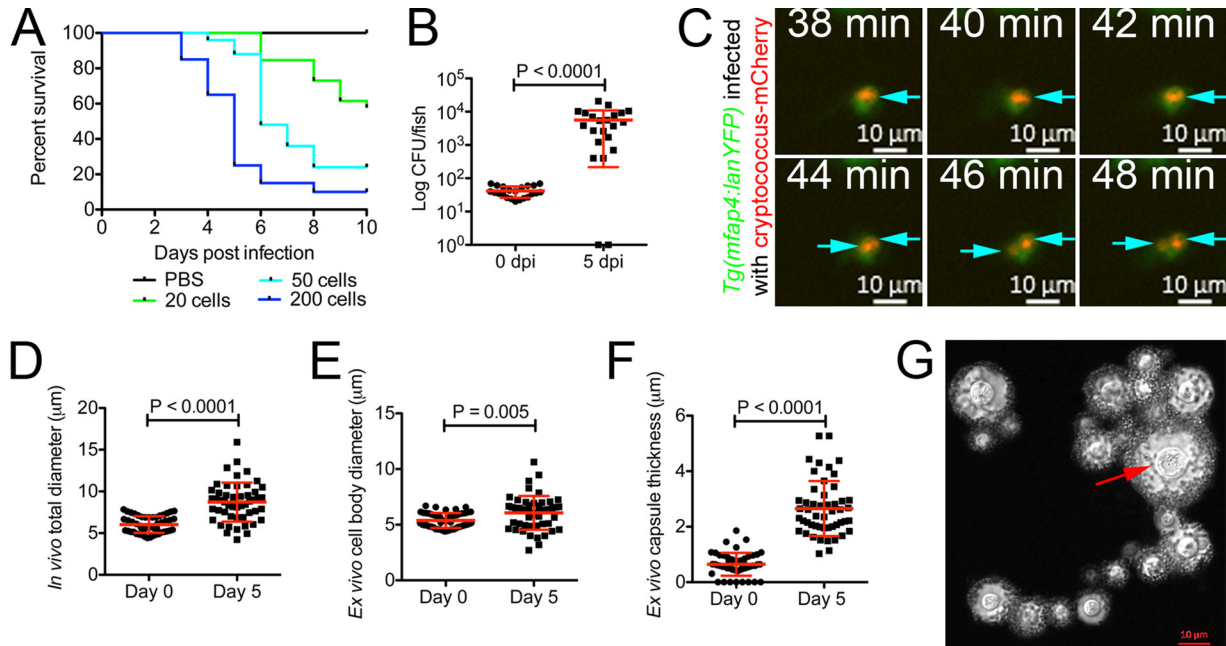
FIG 2 Cryptococcus replicates and causes disease in zebrafish larvae. (A) Survival of zebrafish larvae infected with a range of *C. neoformans* doses. Data are representative of two experiments each with 15 to 20 larvae per experimental condition. (B) *C. neoformans* burden at 0 and 5 days postinfection in larvae infected with a dose of 50 CFU. Data are representative of two experiments, each with at least 20 larvae per experimental condition. *t* test with Welch's correction. (C) Still images from time-lapse imaging of a *Tg(mfap4:lanYFP)* larva infected with mCherry-expressing *C. neoformans* starting at 1 day postinfection (macrophages in green and *Cryptococcus* in red) (full video available as Movie S5 in the supplemental material). Arrows indicate individual yeast cells throughout the time series, with replication appearing to occur between 42 and 44 min. (D) Cryptococcal diameter measured by transmitted light microscopy from the starting inoculum and yeast cells isolated from 5-dpi larvae. *t* test with Welch's correction. (E) Cell body diameter measured from India-ink-stained *C. neoformans* from the starting inoculum and yeast cells isolated from 5-dpi larvae. *t* test with Welch's correction. (F) Capsule thickness measured from India-ink-stained *C. neoformans* from the starting inoculum and yeast cells isolated from 5-dpi larvae. *t* test with Welch's correction. (G) Image of *C. neoformans* isolated from homogenized 5-dpi larvae contrasted by standard India ink preparation. The red arrow indicates a large yeast cell measured at 10 μm representative of observed giant cells recovered from zebrafish infections.

minants, we infected zebrafish larvae with several *C. neoformans* mutants chosen for their description as virulence or fitness factors in mice to verify that the zebrafish infection model recapitulates findings from standard vertebrate models. (i) Capsule formation is a characterizing feature of cryptococcus that becomes enlarged within specific sites within the host and is essential for human disease production. The capsule surrounds the cell wall and is a critical virulence factor with a multitude of effects in the host, including preventing phagocytosis by macrophages (16). *cap64* is a key capsule formation gene: deletion of this gene, *cap64Δ*, has been reported to compromise capsule formation and cryptococcal virulence in mammals (20). (ii) *PLB1* encodes a secreted phospholipase B that may function in multiple processes that contribute to disease within the host, including survival in macrophages and/or possible nutrient acquisition through breakdown of host phospholipids of the phagosome, and the *plbl Δ* deletion mutant is avirulent in the murine system (21, 22). (iii) The ability to adapt to growth at 37°C is a common attribute of all human pathogens. The trehalose pathway is critical for the ability of this yeast to grow at 37°C (23, 24). The examined *tps1Δ* strain lacks the ability to produce trehalose and is unable to survive at high temperatures *in vitro* and *in vivo* (23, 25). *In vivo*, the *tps1Δ* strain is rapidly cleared from infected mice. However, the *tps1Δ* mutant is also avirulent in the *C. elegans* model system (25), suggesting roles beyond adaptation to elevated temperatures since *C. elegans* is maintained at room temperature. (iv) *URE1* encodes a urease enzyme that has

been shown to promote cryptococcal survival by altering the host immune response to pulmonary infections and to increase the rate of hematogenous dissemination in mice (24, 26–28). However, the *urel Δ* mutant survives normally when directly inoculated into the CNS of rabbits and mice (26, 28). Additionally, there are several documented cases of atypical urease-negative isolates causing serious disease in AIDS patients, suggesting that urease could be a site-specific virulence factor (29, 30).

Compared to larvae infected with the H99 (wild-type) strain, larvae infected with each of the four mutant strains survived better in an 8-day survival study, suggesting that these virulence factors are conserved between mammalian and teleost cryptococcal infection (Fig. 3A). We next examined fungal burden in 5-dpi larvae, prior to the divergence of mutant survival rates from wild-type survival rates, to determine if the increased survival of these mutants was caused by reduced cryptococcal proliferation (Fig. 3B). We observed significantly reduced cryptococcal burden in larvae infected with either the *plb1Δ* or *tps1Δ* mutant strain, confirming a range of roles for these virulence factors in cryptococcal pathogenesis across a broad range of host species. Interestingly, like other invertebrate models, the *tps1Δ* mutation showed that its impact on virulence or fitness was due to more than its importance in high-temperature (37°C) growth since zebrafish larvae are incubated at 32°C.

On the other hand, despite survival attenuation of the host, burdens in larvae infected with either *cap64Δ* or *ure1Δ* mutants
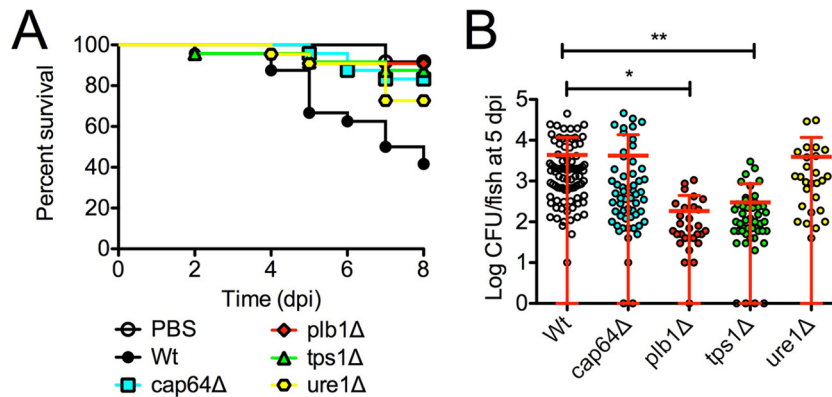
FIG 3 Cryptococcal mutant phenotypes are recapitulated in zebrafish larvae. (A) Survival of zebrafish larvae infected with mutant strains of *C. neoformans*. Data are representative of two experiments, each with 22 larvae per *C. neoformans* genotype. Log-rank test between mutant and wild-type genotypes, *cap64*Δ, $P = 0.003$; *plb1*Δ, $P = 0.0007$; *tps1*Δ, $P = 0.001$; *ure1*Δ, $P = 0.03$. (B) *C. neoformans* burden at 5 days postinfection in larvae infected with mutant strains of *C. neoformans* H99. Data are pooled from 3 experiments, each with at least 15 larvae per *C. neoformans* genotype. One-way ANOVA with Tukey's posttest. *, $P < 0.05$; **, $P < 0.01$.

were comparable to those of larvae infected with the H99 strain. These findings suggest larval zebrafish are either more tolerant of these mutants, the site of critical infection may be different, or the larvae are able to curtail the growth of these mutants just below a lethal threshold of yeast burden, resulting in increased survival at the later time points. This model system can recapitulate the mammalian virulence composite in either fungal burden or survival times with well-characterized cryptococcal mutants.

A zebrafish assay for brain invasion. Invasion of the CNS is a major component of microbial pathogenesis; however, direct determination of rates of microbial brain invasion in mammalian infection models is intrinsically laborious, and comparable structures are not present in the invertebrate model organisms (27). Zebrafish possess a functional blood-brain barrier that is first established at 3 dpf and then matures over the next week of development (31, 32). We took advantage of the optical transparency of the zebrafish head to perform a noninvasive live-imaging assay for cryptococcal invasion of the brain parenchyma from the bloodstream of *Tg(kdrl:EGFP)^s843* animals, where the blood vessels are marked by EGFP expression (Fig. 4A). In a procedural equivalent to mouse tail vein injections, transgenic 2-dpf zebrafish were infected with *C. neoformans* by caudal vein microinjection, resulting in colonization of the cranial vasculature, the brain ventricles, and brain tissue by 4 dpi (Fig. 4B).

We next switched from a conventional lateral imaging orientation to a dorsal orientation to better define the bloodstream, brain ventricle, and brain parenchyma compartments where *C. neoformans* resides (Fig. 4C). By observing a number of animals with different levels of cryptococcal burden in cerebral blood vessels, we found a positive correlation between local infection burden levels of cranial vessels versus invasion into the brain parenchyma (Fig. 4D).

We performed time-lapse imaging of the cranial vasculature, macrophages, and yeast cells in double transgenic *Tg(kdrl:EGFP^s843*, *mfap4:turquoise^xt27*) larvae hematogenously infected with *C. neoformans*. By 4 dpi, we were able to observe intramacrophage and extracellular *C. neoformans* cells free in circulation and lodged in the vasculature (Fig. 5A; see Movie S6 in the supplemental material). Close examination of these apparently extracellular circulating yeast cells revealed a circular zone of vascular distention

around many yeast cells consistent with the production of capsule and avoidance of phagocytosis.

Further imaging also identified invasive *C. neoformans* cells lodged in the brain tissue in double transgenic *Tg(kdrl:EGFP^s843*, *mfap4:turquoise^xt27*) larvae (Fig. 5B). Brain-tissue-resident yeast cells that were at this point outside macrophages did not elicit a strong macrophage migration or phagocytosis (see Movie S7 in the supplemental material). Furthermore, brain-tissue-resident yeast cells that were contained in *mfap4*-expressing macrophages generally remained static throughout imaging. This was in striking contrast to the tissue-resident yeast cells in earlier experiments that were carried by migrating macrophages or formed the focus of nascent granulomas, suggesting that extracellular yeast cells in zebrafish brain tissue may be masked from zebrafish macrophages through previously documented mechanisms, such as capsule production early in infection.

Recapitulation of a known blood-brain barrier invasion-deficient mutant phenotype in mice. Since the blood-brain barrier has not reached full maturation by the end of our experimental window, we wished to functionally assess the blood-brain barrier in the context of a mutant known to be deficient in invasion of the mouse blood-brain barrier. The *C. neoformans fnx1*Δ mutant is deficient for a multidrug resistance-like protein that may facilitate yeast-endothelial cross talk. This mutant was previously characterized as having a deficiency in a competitive murine blood-brain barrier transmigration assay and *in vitro* reduced microvascular entrapment and transcytosis across immortalized human brain capillary endothelial cells (33).

Transgenic *Tg(kdrl:EGFP)^s843* zebrafish larvae were infected with either the *fnx1*Δ mutant strain or the parental CMO18 strain. We did not observe any obvious differences in infection burden until around 4 to 5 dpi, when we observed frequent brain ventricle fungal overgrowth only in animals infected with the *fnx1*Δ mutant (Fig. 6A and B; see Movies S8 and S9 in the supplemental material). We quantified the appearance of the ventricle overgrowth phenotype in 5-dpi larvae and found that infection with the *fnx1*Δ mutant resulted in ventricle colonization at a rate over 4× that of the parental strain (Fig. 6C).

Strikingly, despite clearly having a much higher burden of *C. neoformans* around the brain in larvae infected with the *fnx1*Δ
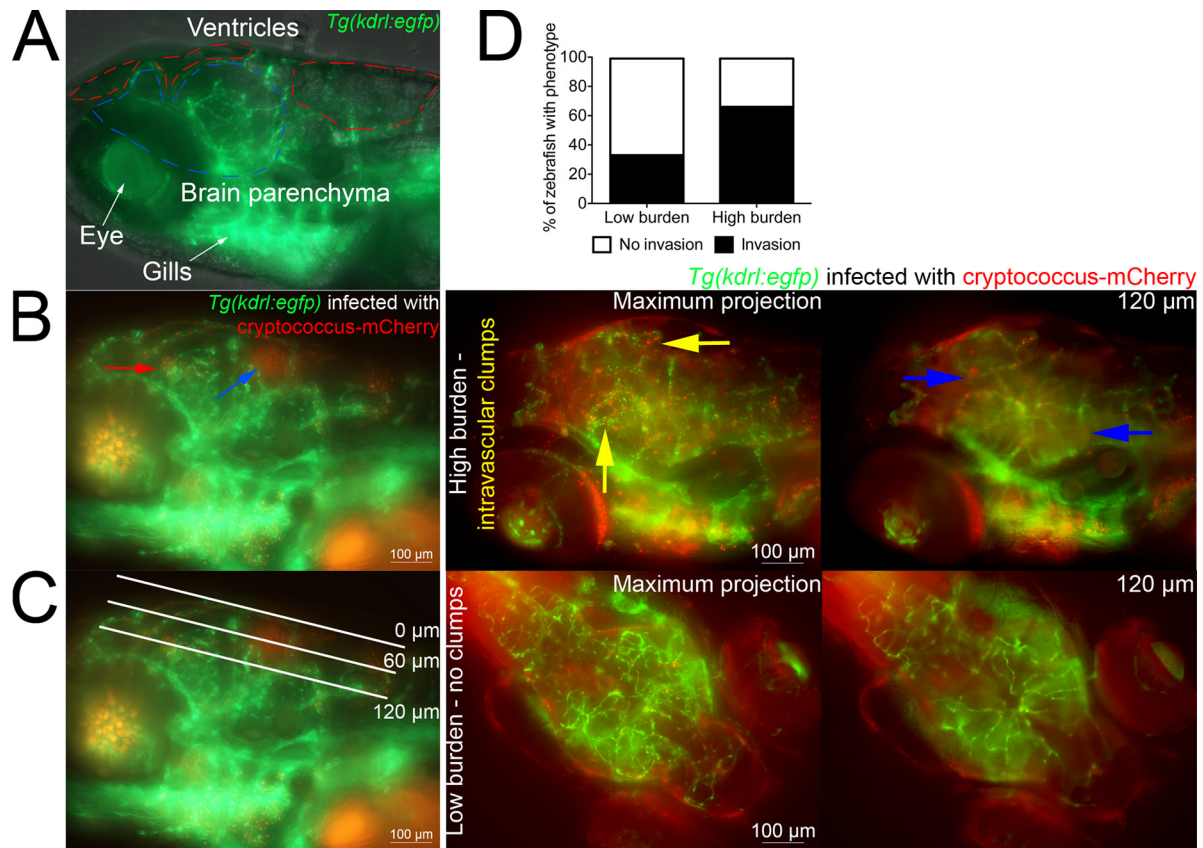
FIG 4 Assessment of cryptococcal brain tissue invasion in zebrafish larvae. (A) Lateral z axis projection of the head of an uninfected 6-dpf *Tg(kdrl:EGFP)*[s843] larva (blood vessels in green). The boundaries of the ventricles and brain parenchyma are marked by red and blue dashed lines, respectively. (B) Lateral z-axis projection of the head of a 4-dpi *Tg(kdrl:EGFP)*[s843] larva (blood vessels in green and *Cryptococcus* in red). The blue arrow indicates *C. neoformans* colonization of hindbrain ventricle, and the red arrow indicates *C. neoformans* in the brain parenchyma. (C) Lateral z-axis projection of the head of a 4-dpi *Tg(kdrl:EGFP)*[s843] larva (blood vessels in green and *Cryptococcus* in red). White lines indicate the approximate depth of optical sections used throughout Fig. 4 and 6. The 0-μm edge is stereotypically set at the dorsal-most blood vessel, and a 60-μm depth stereotypically traverses ventricle spaces dorsal to the brain tissue, which is reached at around 100 to 120 μm in depth. (D) Comparison of *C. neoformans* brain tissue invasion rates between larvae with sporadic colonization of cranial vasculature (low burden) and larvae with clumps of yeast cells within cranial vasculature (high burden). In example images, blood vessels are in green and *Cryptococcus* is in red. Yellow arrows in example images indicate clumps of intravascular yeast, and blue arrows indicate extravasated yeast in the brain tissue.

mutant, we observed a markedly reduced rate of cranial blood vessel colonization by the *fnx1*Δ mutant consistent with *in vitro* assays of microvascular entrapment (Fig. 6D).

Correlating with the reduced rate of cranial vascular localization, we observed a lower rate of brain tissue invasion by the *fnx1*Δ mutant than in the CMO18 parental strain (Fig. 6E). Taken together, these observations confirm a role for FNX1 in aiding the colonization of the cerebral vasculature and promoting the subsequent invasion of the central nervous system across model systems.

DISCUSSION

We have reported multiple assays for applying the highly tractable zebrafish platform as a model of *C. neoformans* pathogenesis. We show that the innate immune system of zebrafish larvae responds to *C. neoformans* primarily with a phagocytic macrophage response that is essential for containing an acute infection. Virulence and disease progression in the zebrafish model are dependent on conserved cryptococcal processes, including pathways related to the evasion of the host immune response. The live-imaging assay systems we have described will provide a novel plat-

form for investigating the intersection of cryptococcal and host genetics and cell behaviors in intact vertebrates.

Our imaging experiments tracking fluorescently labeled innate immune cells and *C. neoformans* cells confirmed that, as predicted from murine experiments, zebrafish macrophages are the dominant phagocytic cell type that interacts with and contains *C. neoformans* during acute infection (13). Our observations also demonstrate a conserved host response driven by macrophages resulting in nascent cryptococcomas in zebrafish larvae infected with *C. neoformans* even during our relatively short window of infection. Although this macrophage predominance is a fairly common response to microbial infection in zebrafish, differential roles have been observed for macrophages and neutrophils in containing fungal infections in zebrafish (34, 35). The primary response also includes macrophage aggregates consistent with the granulomas observed in mammals. It will be intriguing to determine if the postulated immunomodulatory role of neutrophils in acute murine *C. neoformans* infections is conserved across species by further live imaging of the dynamic immune response of zebrafish larvae manipulated to have high or low numbers of neutrophils.
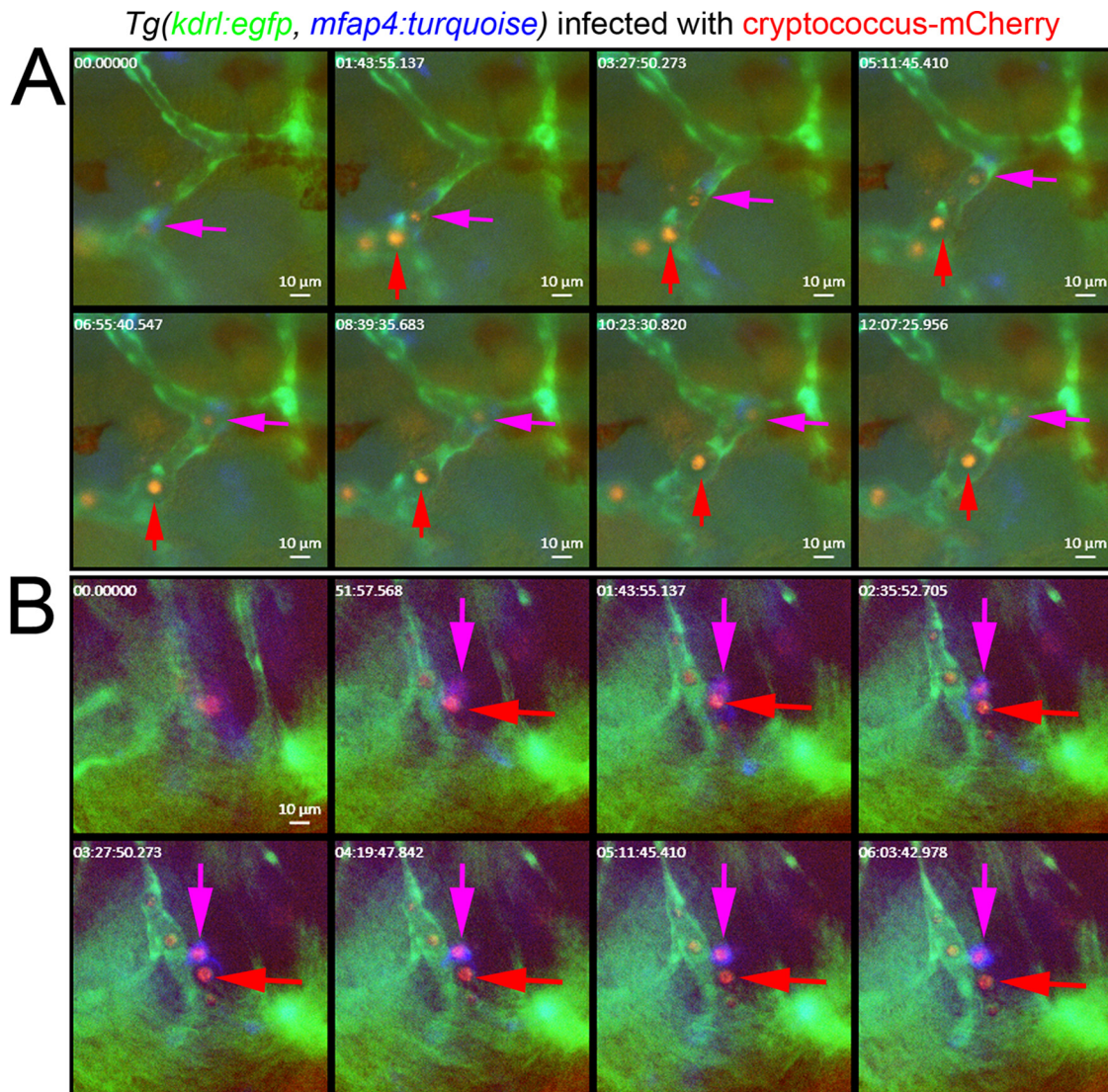
FIG 5 (A) Still images from the brain of a 5-dpi *Tg*(*kdrl*:*EGFP*^*s843*^, *mfap4*:*turquoise*^*xt27*^) larva infected with mCherry-expressing *C. neoformans* by caudal vein injection (blood vessels in green, macrophages in blue, and *Cryptococcus* in red). The full time-lapse video is available as Movie S7 in the supplemental material. A purple arrow indicates a macrophage with phagocytosed yeast cells moving inside cranial blood vessels. A red arrow indicates presumptively extracellular yeast cells moving inside cranial blood vessels. Note the nonfluorescent area of vessel distension that follows presumptively extracellular yeast cells. (B) Still images from the brain of a 5-dpi *Tg*(*kdrl*:*EGFP*^*s843*^, *mfap4*:*turquoise*^*xt27*^) larva infected with mCherry-expressing *C. neoformans* by caudal vein injection (blood vessels in green, macrophages in blue, and *Cryptococcus* in red). Full time-lapse imaging is available as Movie S7 in the supplemental material. A purple arrow indicates a macrophage with a phagocytosed yeast cell located in brain tissue adjacent to cranial blood vessel. A red arrow indicates a presumptively extracellular yeast cell located in brain tissue.

The visual accessibility of the zebrafish larvae also allowed us the opportunity to visualize intramacrophage yeast cell division *in vivo*, demonstrating that *C. neoformans* is able to replicate inside zebrafish macrophages. Since effective chemotherapy for invasive *C. neoformans* can lead to dangerous sequelae due to the massive release of fungal immunostimulants and development of immune reconstitution inflammatory syndrome (IRIS), there is a need to better characterize and modulate the host response to fungal pathogens. As demonstrated by our Spi1 knockdown study and by others, including Brothers et al., the zebrafish host is amenable to genetic manipulation to identify the host factors necessary for combating and controlling fungal pathogenesis (34). The zebrafish may thus present a tractable tool for investigating the role

of specific host factors that recognize and respond to general and virulence-specific cryptococcal factors.

C. neoformans has been observed to physically respond to the infection milieu by enlarging both capsule and overall yeast cell size. We also observed the presence of large cells, also termed Titan or giant cells during zebrafish infection, with yeast cells above 10 μm in size. It is posited that these large cells are important in the early stages of infection as a means to avoid engulfment by immune cells and demonstrate the stress that these yeast cells are undergoing in the host (15). To clearly define the large cells as Titan/giant cells, additional characterization is needed to evaluate the genomic content, cell wall thickness, and overall size. However, the high fecundity of zebrafish should provide an excellent *in*
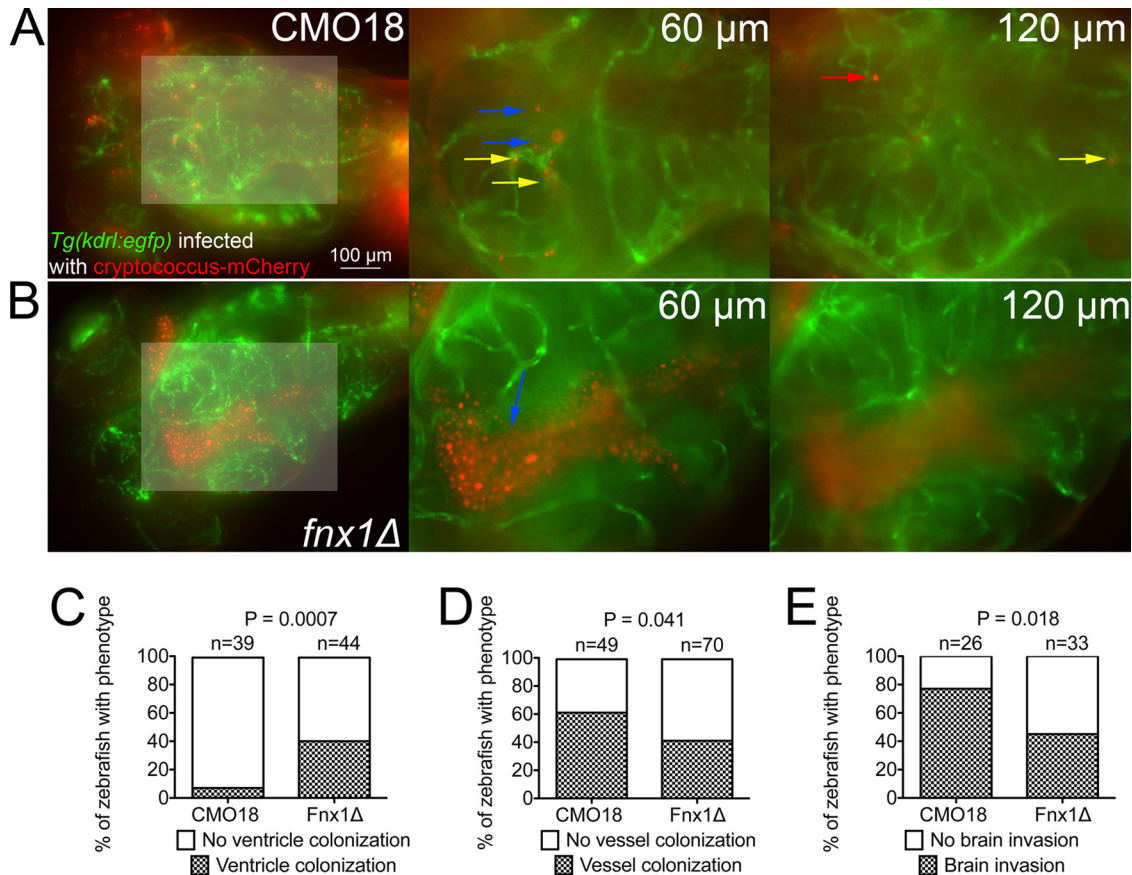
FIG 6 The *C. neoformans fnx1*Δ mutant strain is deficient in invading the brain parenchyma. (A) Dorsal-viewpoint images taken from a *z*-axis stack of a 5-dpi *Tg*(*kdrl*:EGFP^{s843}) larva infected with an mCherry-expressing *C. neoformans* CMO18 strain by caudal vein injection (left). Shown is a *z*-axis projection with a lightened box indicating a magnified region of interest (shown to the right) of 2× digital magnification slices at ventricle (60-μm) and brain tissue (120-μm) depths of focus. Blue arrows indicate *C. neoformans* cells located in the brain ventricle, red arrows indicate *C. neoformans* cells located in the brain parenchyma, and yellow arrows indicate *C. neoformans* cells located in the cranial vessels. Distances indicate the depth of image plane from the dorsal edge of the head. The full stack is available as Movie S8 in the supplemental material. (B) Dorsal-viewpoint images taken from a *z*-axis stack of a 5-dpi *Tg*(*kdrl*:EGFP^{s843}) larva infected with an mCherry-expressing *C. neoformans fnx1*Δ mutant by caudal vein injection (left). Shown is a *z* axis projection with a lightened box indicating the magnified region of interest (shown to the right) of 2× digital magnification slices at ventricle (60-μm) and brain tissue (120-μm) depths of focus. Blue arrows indicate *C. neoformans* cells located in the brain ventricle. Distances indicate depths of the image planes from the dorsal edge of the head. The full stack is available as Movie S9 in the supplemental material. (C) Quantification of head ventricle *C. neoformans* colonization in 4-dpi larvae infected with the *C. neoformans fnx1*Δ mutant by caudal vein injection. Fisher's exact test. Data are pooled from 3 replicates each with 10 to 20 larvae per genotype. (D) Quantification of cranial blood vessel *C. neoformans* colonization in 5-dpi larvae infected with the *C. neoformans fnx1*Δ mutant by caudal vein injection. Fisher's exact test. Data are pooled from 4 replicates each with 10 to 20 larvae per genotype. (E) Quantification of brain tissue invasion in 5-dpi larva infected with the *C. neoformans fnx1*Δ mutant by caudal vein injection. Fisher's exact test. Data are pooled from 3 replicates each with 10 to 20 larvae per genotype.

vivo platform for harvesting and defining whether these large cells that we have observed are truly Titan/giant cells. Furthermore, the live-imaging capacity of the zebrafish platform provides a unique system to image the interaction between Titan/giant cells and specific elements of the host innate immune system.

The reproduction of increased host survival in zebrafish larvae infected with several *C. neoformans* mutants from independent virulence pathways demonstrates that known virulence pathways are conserved during infection of this nonmammalian vertebrate host. These experiments set an important proof of principle and suggest that investigation of mutant interactions with the immune system *in vivo* by live imaging will be feasible to aid our understanding of how cryptococcal virulence pathways promote pathogenesis. The magnitude of the burden differences in the mutants may be limited by the short time frame over which we performed the zebrafish larval infections. Modifying the inoculum and ex-

tending the duration of infection for burden analysis might reveal larger absolute burden differences and additional congruence between the model systems used.

The discrepancy between the increased survival of the *cap64*Δ and *ure1*Δ mutants compared to the wild-type strain and the similar fungal burdens of all three genotypes at 5 dpi was surprising as mortality had previously appeared to be tightly associated with fungal overgrowth in our dose-response infections. We speculate that this discrepancy could be caused by reduced immunopathology following infection with these mutants resulting in an uncoupling of the burden-mortality relationship. Another hypothesis is that the growth of these mutants is controlled at the 5-dpi time point by a host immune response that is either independent of or a slower version of the response that rapidly controls the *plb1*Δ and *tps1*Δ mutants. Alternatively, the mutants may have body site differences in growth and entry—exemplified by the normal

growth of the *ure1Δ* mutant when directly inoculated into the mammalian CNS (26, 28). Thus, we postulate that studying a range of mutants in the zebrafish model will be useful to better understand the contribution of certain virulence pathways to cryptococcal pathogenesis, and we can watch these yeasts in real time as they produce disease.

CNS involvement is an important stage of *C. neoformans* pathogenesis that has severe consequences for the host. The zebrafish is an emerging model for the study of blood-brain barrier development and function (36, 37). Here, we have demonstrated that *C. neoformans* migrates to the CNS of larval zebrafish and that a cryptococcal mutant known to be defective in mammalian blood-brain barrier invasion is also defective in invading the zebrafish brain. Since many of the *fnx1Δ* mutant animals displaying the vesicle overgrowth phenotype did not have colonization of their cranial blood vessels, we hypothesize that ventricle colonization may utilize a different fungal pathogenicity program than the blood-brain barrier.

Future investigation will be designed to image invasion events *in vivo* to answer the important question of if and why infected blood-borne macrophages would migrate across the blood-brain barrier—is it an inbuilt macrophage program triggered by *C. neoformans* (i.e., the Trojan Horse hypothesis)? Alternatively, live imaging may reveal the blood-brain barrier invasion in zebrafish to be a consequence of having a large accumulation of yeast cells in the blood compartment resulting in transcytosis across the barrier or simply bursting of the vessel into the brain. The platform described here can be readily applied to studying a range of laboratory-generated mutants and clinical/environmental isolates to rapidly identify cryptococcal determinants of CNS pathology as well as the cellular mechanisms of CNS invasion.

MATERIALS AND METHODS

Zebrafish (*Danio rerio*) husbandry. All zebrafish husbandry and experimental procedures were performed in accordance and compliance with policies approved by the Duke University Institutional Animal Care and Use Committee (protocol A180-11-07). Clutches of eggs were collected from natural spawning and raised in filtered fish system water at 28°C. Pigment development was halted in 1-dpf embryos by the addition of 1-phenyl-2-thiourea (PTU [final concentration, 45 μg/ml]) (Sigma-Aldrich, St. Louis, MO). Other strains used in this study include those with the genotpes Tg(*lyzC:EGFP*)^{nz117}, Tg(*kdrl:EGFP*)^{s843}, Tg(*mfap4:turquoise*)^{xt27}, and Tg(*mpeg1:lanYFP*)^{xt2}.

Labeling of cryptococcus strains. Labeling of the *Cryptococcus* strains was performed by biolistic transformation of plasmid pCN52 or pCN53 containing a *mCherry-RAS1* fusion (38). Random integration of this reporter was performed by selection on yeast extract-peptone-dextrose (YPD) containing 100 μg/ml nourseothricin (NAT; Werner BioAgents, Jena-Cospeda, Germany) or 200 μg/ml Geneticin (NEO; Thermo, Fisher Scientific, Grand Island, NY). The *Cryptococcus neoformans* var. *grubii* H99 *GFP-RAS1* and H99 *mCherry-RAS1* strains were kindly provided by Connie Nichols.

C. neoformans var. grubii strains and growth conditions. Strains used in this study include wild-type H99 and CM108, and the *tps1Δ* (25), *cap64Δ* (39), *ure1Δ* (28), *plb1Δ* (21), and *fnx1Δ* (33) mutants (33, 40). A single colony of each strain was inoculated into 5 ml YPD and grown overnight at 30°C with shaking at 225 rpm. Cells were harvested by centrifugation for 5 min at 3000 rpm, washed twice with 25 ml PBS, and suspended in 1 ml phosphate-buffered saline (PBS). A dose of 7 × 10^7 CFU/ml was prepared to achieve a cell count of ~50 cells per injection. Injected larvae were screened postinjection to confirm the injection dose. Doses ranging from 3 × 10^7 to 8 × 10^7 CFU/ml were prepared for the dose

curve experiment to achieve the appropriate number of yeast cells for inoculation.

Infection by microinjection. Embryos were anesthetized at 2 dpf with tricaine (MS-222; Sigma-Aldrich, St. Louis, MO) (final concentration, 160 μg/ml) and injected with *C. neoformans* in an injection bolus of 10 to 20 nl into the caudal vein. Infected embryos were then recovered back to filtered fish system water supplemented with PTU and raised at 32°C as an intermediate temperature between standard zebrafish (28°C) and cryptococcal (37°C) growth temperatures that is above ambient temperature and well tolerated by larval zebrafish. Embryos that were physically damaged by injection handling were discarded and excluded from further analysis.

Live imaging. Conventional microscopy and time-lapse fluorescence microscopy were carried out on a Zeiss observer Z1 inverted microscope. Embryos were anesthetized with 160 μg/ml tricaine and mounted in 3% (wt/vol) methylcellulose or 1% low-melting-point agarose for static microscopy. Embryos for time-lapse microscopy were anesthetized with 120 μg/ml tricaine, mounted in 0.75% low-melting-point agarose containing between 100 and 140 μg/ml tricaine in 96-well plates, and immersed in filtered fish system water supplemented with PTU. Images were processed with ImageJ (NIH) and Photoshop CS4 (Adobe).

Morpholino knockdown. Modified antisense oligonucleotides designed to knock down expression of Spi1 were injected into 1- to 4-cell-stage embryos. The sequences of the morpholinos used in this study are as follows: Spi1 morpholino sequence, 5′ GATATACTGATACTCCATTG-GTGGT 3′, and control morpholino, 5′ CCTCTTACCTCAGTTA-CAATTTATA 3′. Morpholinos were injected at either 1 or 10 pmol per embryo.

Recovery of C. neoformans for capsule size measurement. Zebrafish were euthanized in fish water containing 300 μg/ml tricaine, washed 2 times with PBS, and transferred individually to a 2-ml screw-cap tube with an O-ring. To each tube, a 6.35-mm steel bead and 1 ml of PBS were added. Fish were homogenized by a 15-s pulse using a Mini-Beadbeater-16 (BioSpec Products). To isolate *Cryptococcus* cells for imaging of capsule and cell size, a monoclonal antibody (kindly provided by Arturo Casadevall) was labeled with goat anti-mouse IgG magnetic beads (New England Biolabs catalog no. S1431S) according to the manufacturer's instructions. The magnetic beads coated with the 18B7 antibody were diluted such that few beads were observed per yeast cell. The magnetic beads were incubated with the fish lysate at room temperature for 5 min, and beads were separated to the side of the tube for 5 min. The lysate was removed, and beads were washed 3 times with 1 ml of PBS. The beads were resuspended in 20 μl of PBS. Samples were prepared with India ink staining and imaged on a Zeiss Axio Imager A1 microscope with an AxioCam MRM digital camera. Image analysis was performed using ImageJ software.

Quantification of morpholino hematopoietic effects. Morpholino-injected Tg(*lyzC:EGFP*)^{nz101} embryos were raised to 3 dpf, soaked in 2.5 μg/ml neutral red (Sigma-Aldrich, St. Louis, MO) for 6 h, and imaged for red and green fluorescence.

Enumeration of CFU. Zebrafish were euthanized in fish water containing 300 μg/ml tricaine, washed 2 times with 25 ml PBS, and transferred individually to a 2-ml screw-cap tube with an O-ring. To each tube, a 6.35-mm steel bead (BioSpec Products, Bartlesville, OK) and 1 ml of PBS were added. Fish were homogenized by a 15-s pulse using a Mini-Beadbeater-16 (BioSpec Products, Bartlesville, OK). Serial dilutions were performed, and 100 μl of the neat solution and 1/10 dilutions were plated onto YPD containing 100 μg/ml chloramphenicol. Plates were incubated at 30°C for 3 days. Colonies were enumerated after 3 days of growth.

Statistical analysis. Comparison of fungal burdens was performed using unpaired two-tailed *t* test. Values resulting in *P* values of <0.05 relative to the control were considered significantly different. Zebrafish survival was plotted using Kaplan-Meier survival curves and analyzed by log rank test using GraphPad Prism. Survival curves resulting in *P* values

of <0.05 relative to the control were considered significantly different. Error bars represent 1 standard deviation.

SUPPLEMENTAL MATERIAL

Supplemental material for this article may be found at http://mbio.asm.org/lookup/suppl/doi:10.1128/mBio.01425-15/-/DCSupplemental.

Movie S1, AVI file, 6.1 MB.
Movie S2, AVI file, 7.8 MB.
Movie S3, AVI file, 3.5 MB.
Movie S4, AVI file, 6.6 MB.
Movie S5, AVI file, 0.3 MB.
Movie S6, AVI file, 0.2 MB.
Movie S7, AVI file, 0.1 MB.
Movie S8, AVI file, 1.6 MB.
Movie S9, AVI file, 1.4 MB.

ACKNOWLEDGMENTS

REFERENCES

1. **Park BJ, Wannemuehler KA, Marston BJ, Govender N, Pappas PG, Chiller TM**. 2009. Estimation of the current global burden of cryptococcal meningitis among persons living with HIV/AIDS. AIDS **23**:525–530. http://dx.doi.org/10.1097/QAD.0b013e328322ffac.

2. **Lee A, Toffaletti DL, Tenor J, Soderblom EJ, Thompson JW, Moseley MA, Price M, Perfect JR**. 2010. Survival defects of *Cryptococcus neoformans* mutants exposed to human cerebrospinal fluid result in attenuated virulence in an experimental model of meningitis. Infect Immun **78**:4213–4225. http://dx.doi.org/10.1128/IAI.00551-10.

3. **Price MS, Betancourt-Quiroz M, Price JL, Toffaletti DL, Vora H, Hu G, Kronstad JW, Perfect JR**. 2011. *Cryptococcus neoformans* requires a functional glycolytic pathway for disease but not persistence in the host. mBio **2**(3):e00103-11. http://dx.doi.org/10.1128/mBio.00103-11.

4. **Feldmesser M, Kress Y, Novikoff P, Casadevall A**. 2000. *Cryptococcus neoformans* is a facultative intracellular pathogen in murine pulmonary infection. Infect Immun **68**:4225–4237. http://dx.doi.org/10.1128/IAI.68.7.4225-4237.2000.

5. **Apidianakis Y, Rahme LG, Heitman J, Ausubel FM, Calderwood SB, Mylonakis E**. 2004. Challenge of *Drosophila melanogaster* with *Cryptococcus neoformans* and role of the innate immune response. Eukaryot Cell **3**:413–419. http://dx.doi.org/10.1128/EC.3.2.413-419.2004.

6. **Desalermos A, Tan X, Rajamuthiah R, Arvanitis M, Wang Y, Li D, Kourkoumpetis TK, Fuchs BB, Mylonakis E**. 2015. A multi-host approach for the systematic analysis of virulence factors in *Cryptococcus neoformans*. J Infect Dis **211**:298–305. http://dx.doi.org/10.1093/infdis/jiu441.

7. **Mylonakis E, Moreno R, El Khoury JB, Idnurm A, Heitman J, Calderwood SB, Ausubel FM, Diener A**. 2005. *Galleria mellonella* as a model system to study *Cryptococcus neoformans* pathogenesis. Infect Immun **73**:3842–3850. http://dx.doi.org/10.1128/IAI.73.7.3842-3850.2005.

8. **Mylonakis E, Ausubel FM, Perfect JR, Heitman J, Calderwood SB**. 2002. Killing of *Caenorhabditis elegans* by *Cryptococcus neoformans* as a model of yeast pathogenesis. Proc Natl Acad Sci U S A **99**:15675–15680. http://dx.doi.org/10.1073/pnas.232568599.

9. **Tobin DM, May RC, Wheeler RT**. 2012. Zebrafish: a see-through host and a fluorescent toolbox to probe host-pathogen interaction. PLoS Pathog **8**:e1002349. http://dx.doi.org/10.1371/journal.ppat.1002349.

10. **Gratacap RL, Rawls JF, Wheeler RT**. 2013. Mucosal candidiasis elicits activation of NF-kappaB, proinflammatory gene expression and localized neutrophilia in a transparent vertebrate host. Dis Model Mech **6**:1260–1270. http://dx.doi.org/10.1242/dmm.012039.

11. **Hall C, Flores MV, Storm T, Crosier K, Crosier P**. 2007. The zebrafish lysozyme C promoter drives myeloid-specific expression in transgenic fish. BMC Dev Biol **7**:42. http://dx.doi.org/10.1186/1471-213X-7-42.

12. **Oehlers SH, Cronan MR, Scott NR, Thomas MI, Okuda KS, Walton EM, Beerman RW, Crosier PS, Tobin DM**. 2015. Interception of host angiogenic signalling limits mycobacterial growth. Nature **517**:612–615. http://dx.doi.org/10.1038/nature13967.

13. **Voelz K, May RC**. 2010. Cryptococcal interactions with the host immune system. Eukaryot Cell **9**:835–846. http://dx.doi.org/10.1128/EC.00039-10.

14. **Rhodes J, Hagen A, Hsu K, Deng M, Liu TX, Look AT, Kanki JP**. 2005. Interplay of pu.1 and gata1 determines myelo-erythroid progenitor cell fate in zebrafish. Dev Cell **8**:97–108. http://dx.doi.org/10.1016/j.devcel.2004.11.014.

15. **Okagaki LH, Strain AK, Nielsen JN, Charlier C, Baltes NJ, Chrétien F, Heitman J, Dromer F, Nielsen K**. 2010. Cryptococcal cell morphology affects host cell interactions and pathogenicity. PLoS Pathog **6**:e1000953. http://dx.doi.org/10.1371/journal.ppat.1000953.

16. **Zaragoza O, Rodrigues ML, De Jesus M, Frases S, Dadachova E, Casadevall A**. 2009. The capsule of the fungal pathogen *Cryptococcus neoformans*. Adv Appl Microbiol **68**:133–216. http://dx.doi.org/10.1016/S0065-2164(09)01204-0.

17. **Carvalho R, de Sonneville J, Stockhammer O, Savage ND, Veneman WJ, Ottenhoff TH, Dirks RP, Meijer AH, Spaink HP**. 2011. A high-throughput screen for tuberculosis progression. PLoS One **6**:e16779. http://dx.doi.org/10.1371/journal.pone.0016779.

18. **Tobin DM, Vary JC, Jr, Ray JP, Walsh GS, Dunstan SJ, Bang ND, Hagge DA, Khadge S, King MC, Hawn TR, Moens CB, Ramakrishnan L**. 2010. The lta4h locus modulates susceptibility to mycobacterial infection in zebrafish and humans. Cell **140**:717–730. http://dx.doi.org/10.1016/j.cell.2010.02.013.

19. **Wiles TJ, Norton JP, Russell CW, Dalley BK, Fischer KF, Mulvey MA**. 2013. Combining quantitative genetic footprinting and trait enrichment analysis to identify fitness determinants of a bacterial pathogen. PLoS Genet **9**:e1003716. http://dx.doi.org/10.1371/journal.pgen.1003716.

20. **Chang YC, Penoyer LA, Kwon-Chung KJ**. 1996. The second capsule gene of *Cryptococcus neoformans*, CAP64, is essential for virulence. Infect Immun **64**:1977–1983.

21. **Cox GM, McDade HC, Chen SC, Tucker SC, Gottfredsson M, Wright LC, Sorrell TC, Leidich SD, Casadevall A, Ghannoum MA, Perfect JR**. 2001. Extracellular phospholipase activity is a virulence factor for *Cryptococcus neoformans*. Mol Microbiol **39**:166–175. http://dx.doi.org/10.1046/j.1365-2958.2001.02236.x.

22. **Chrisman CJ, Albuquerque P, Guimaraes AJ, Nieves E, Casadevall A**. 2011. Phospholipids trigger *Cryptococcus neoformans* capsular enlargement during interactions with amoebae and macrophages. PLoS Pathog **7**:e1002047. http://dx.doi.org/10.1371/journal.ppat.1002047.

23. **Ngamskulrungroj P, Himmelreich U, Breger JA, Wilson C, Chayakulkeeree M, Krockenberger MB, Malik R, Daniel HM, Toffaletti D, Djordjevic JT, Mylonakis E, Meyer W, Perfect JR**. 2009. The trehalose synthesis pathway is an integral part of the virulence composite for *Cryptococcus gattii*. Infect Immun **77**:4584–4596. http://dx.doi.org/10.1128/IAI.00565-09.

24. **Osterholzer JJ, Surana R, Milam JE, Montano GT, Chen GH, Sonstein J, Curtis JL, Huffnagle GB, Toews GB, Olszewski MA**. 2009. Cryptococcal urease promotes the accumulation of immature dendritic cells and a non-protective T2 immune response within the lung. Am J Pathol **174**:932–943. http://dx.doi.org/10.2353/ajpath.2009.080673.

25. **Petzold EW, Himmelreich U, Mylonakis E, Rude T, Toffaletti D, Cox GM, Miller JL, Perfect JR**. 2006. Characterization and regulation of the trehalose synthesis pathway and its importance in the pathogenicity of *Cryptococcus neoformans*. Infect Immun **74**:5877–5887. http://dx.doi.org/10.1128/IAI.00624-06.

26. **Olszewski MA, Noverr MC, Chen GH, Toews GB, Cox GM, Perfect JR, Huffnagle GB**. 2004. Urease expression by *Cryptococcus neoformans* promotes microvascular sequestration, thereby enhancing central nervous system invasion. Am J Pathol **164**:1761–1771. http://dx.doi.org/10.1016/S0002-9440(10)63734-0.

27. **Shi M, Li SS, Zheng C, Jones GJ, Kim KS, Zhou H, Kubes P, Mody CH**. 2010. Real-time imaging of trapping and urease-dependent transmigra-

tion of *Cryptococcus neoformans* in mouse brain. J Clin Invest **120:** 1683–1693. http://dx.doi.org/10.1172/JCI41963.

28. **Cox GM, Mukherjee J, Cole GT, Casadevall A, Perfect JR.** 2000. Urease as a virulence factor in experimental cryptococcosis. Infect Immun **68:** 443–448. http://dx.doi.org/10.1128/IAI.68.2.443-448.2000.

29. **Bava AJ, Negroni R, Bianchi M.** 1993. Cryptococcosis produced by a urease negative strain of *Cryptococcus neoformans*. J Med Vet Mycol **31:** 87–89. http://dx.doi.org/10.1080/02681219380000091.

30. **Ruane PJ, Walker LJ, George WL.** 1988. Disseminated infection caused by urease-negative *Cryptococcus neoformans*. J Clin Microbiol **26:** 2224–2225.

31. **Xie J, Farage E, Sugimoto M, Anand-Apte B.** 2010. A novel transgenic zebrafish model for blood-brain and blood-retinal barrier development. BMC Dev Biol **10:**76. http://dx.doi.org/10.1186/1471-213X-10-76.

32. **Fleming A, Diekmann H, Goldsmith P.** 2013. Functional characterisation of the maturation of the blood-brain barrier in larval zebrafish. PLoS One **8:**e77548. http://dx.doi.org/10.1371/journal.pone.0077548.

33. **Tseng HK, Liu CP, Price MS, Jong AY, Chang JC, Toffaletti DL, Betancourt-Quiroz M, Frazzitta AE, Cho WL, Perfect JR.** 2012. Identification of genes from the fungal pathogen *Cryptococcus neoformans* related to transmigration into the central nervous system. PLoS One **7:**e45083. http://dx.doi.org/10.1371/journal.pone.0045083.

34. **Brothers KM, Gratacap RL, Barker SE, Newman ZR, Norum A, Wheeler RT.** 2013. NADPH oxidase-driven phagocyte recruitment controls *Candida albicans* filamentous growth and prevents mortality. PLoS Pathog **9:**e1003634. http://dx.doi.org/10.1371/journal.ppat.1003634.

35. **Ellett F, Pase L, Hayman JW, Andrianopoulos A, Lieschke GJ.** 2011. mpeg1 promoter transgenes direct macrophage-lineage expression in zebrafish. Blood **117:**e49–e56. http://dx.doi.org/10.1182/blood-2010-10-314120.

36. **Kim BJ, Hancock BM, Bermudez A, Del Cid N, Reyes E, van Sorge NM, Lauth X, Smurthwaite CA, Hilton BJ, Stotland A, Banerjee A, Buchanan J, Wolkowicz R, Traver D, Doran KS.** 2015. Bacterial induction of Snail1 contributes to blood-brain barrier disruption. J Clin Invest **125:** 2473–2483. http://dx.doi.org/10.1172/JCI74159.

37. **van Leeuwen LM, van der Kuip M, Youssef SA, de Bruin A, Bitter W, van Furth AM, van der Sar AM.** 2014. Modeling tuberculous meningitis in zebrafish using *Mycobacterium marinum*. Dis Model Mech **7:**1111–1122. http://dx.doi.org/10.1242/dmm.015453.

38. **Selvig K, Ballou ER, Nichols CB, Alspaugh JA.** 2013. Restricted substrate specificity for the geranylgeranyltransferase-I enzyme in *Cryptococcus neoformans*: implications for virulence. Eukaryot Cell **12:**1462–1471. http://dx.doi.org/10.1128/EC.00193-13.

39. **Moyrand F, Janbon G.** 2004. UGD1, encoding the *Cryptococcus neoformans* UDP-glucose dehydrogenase, is essential for growth at 37°C and for capsule biosynthesis. Eukaryot Cell **3:**1601–1608. http://dx.doi.org/10.1128/EC.3.6.1601-1608.2004.

40. **Liu OW, Chun CD, Chow ED, Chen C, Madhani HD, Noble SM.** 2008. Systematic genetic analysis of virulence in the human fungal pathogen *Cryptococcus neoformans*. Cell **135:**174–188. http://dx.doi.org/10.1016/j.cell.2008.07.046.